

Origin of the Complex Molecular Dynamics in Functionalized Discotic Liquid Crystals

M. M. Elmahdy,¹ G. Floudas,^{1,*} M. Mondeshki,² H. W. Spiess,² X. Dou,² and K. Müllen²

¹Department of Physics, University of Ioannina, 451 10 Ioannina, Greece and Foundation for Research and Technology-Hellas (FORTH), Biomedical Research Institute (BRI), Ioannina, Greece

²Max-Planck Institut für Polymerforschung, D-55021 Mainz, Germany

(Received 14 November 2007; published 14 March 2008)

The molecular dynamics of three dipole functionalized hexa-*peri*-hexabenzocoronenes have been studied using site-specific NMR techniques and dielectric spectroscopy as a function of temperature and pressure. These probes (i) suggest that the thermodynamic state completely controls the dynamic response, (ii) clarify the origin of two dynamic processes associated with the presence of two glass temperatures, and (iii) provide the first phase diagram for substances of this kind.

DOI: 10.1103/PhysRevLett.100.107801

PACS numbers: 61.30.-v, 64.70.P-, 77.84.Nh

Discotic liquid crystals, with potential applications in electronic devices [1], are materials where self-assembly is driven by noncovalent intermolecular interactions [2]. These materials consist of a flat and rigid aromatic core substituted by flexible aliphatic side chains. The former is responsible for the π stacking and the latter for the increased solubility, processability, and rich thermotropic behavior. During the self-organization process, the disc-shaped molecules organize into columns that further assemble into two-dimensional arrays whereas the alkyl chains fill the intercolumnar space giving rise to a naphase separated state [3]. Typical examples of these materials are the triphenylene and hexa-*peri*-hexabenzocoronene (HBC) derivatives. Highly ordered columnar structures of the latter were found to be very promising as active semiconductors in organic field-effect transistors [4] and photovoltaic devices with a charge carrier mobility of up to 1.1 cm²/V s (in HBCs) [5].

For applications such as advanced electronic materials, the intrinsic disc mobility can influence the charge carrier mobility and thus needs to be explored in detail. Earlier efforts through NMR [6–13], dielectric spectroscopy (DS) [11–18], neutron scattering [19,20], and computer simulations [20–22] have shed light on the dynamics. The NMR studies identified (i) the main α process as reflecting the axial motion of the discs around the columnar axis [6,11] and (ii) quasiperiodic regions of high and low packing density along the columns [8] as proposed by de Gennes [23]. Hexabenzocoronenes possess lower order within the columnar mesophase than conventional triphenylenes [9]. In this respect, a study of the molecular dynamics in HBCs over a broad range of frequencies could be more informative.

What is still missing, however, is the assignment of the slower dynamics (pertinent to the long range organization), the origin of the multiple glass temperatures and the complete phase state. Understanding the molecular dynamics requires model systems that allow direct probing of the core dynamics within the columnar stacks by combining microscopic techniques with access to both the time scale

and geometry of motion. Knowledge of the phase state, on the other hand, requires the use of pressure. For this purpose, we study three dipole functionalized HBCs possessing variable dipole moments directly attached to the disc core. At first we investigate the structure and thermotropic behavior. Subsequently, we employ site-specific NMR techniques to study the geometry of motion coupled with temperature (T) and, for the first time, pressure (P) dependent dielectric spectroscopy techniques that provide the corresponding time scales. Finally, these techniques allow constructing the first phase diagram for compounds of this kind.

Three dipole functionalized HBC derivatives (with monocyno, monobromo [24] and monoethynyl, see Fig. 1) were synthesized. The thermal behavior was determined by differential scanning calorimetry (DSC) at 10 K/min revealing the absence of a phase transformation for the monocyno and monobromo compounds within the investigated T range. However a glass temperature was identified at 235 K. Wide-angle x-ray scattering (WAXS) measurements were made on macroscopically oriented (extruded) filaments. DS was employed under “isobaric” conditions as a function of temperature in the range 123.15–423.15 K and under “isothermal” conditions as a function of pressure for pressures up to 300 MPa. In every case the complex dielectric permittivity $\epsilon^* = \epsilon' - i\epsilon''$, where ϵ' is the real and ϵ'' is the imaginary part, was obtained as a function of frequency ω , temperature T , and pressure P , i.e., $\epsilon^*(T, P, \omega)$ [25]. Both T - and P -dependent experiments were analyzed using the empirical equation of Havriliak and Negami as described else-

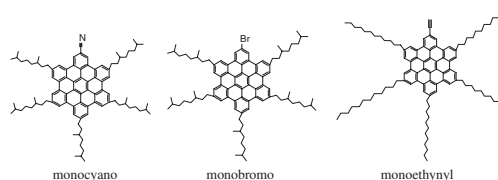


FIG. 1. Schematic structures of the three HBCs investigated.

where [26]. In addition, the ionic mobility was extracted using the electric modulus representation as $M^* = 1/\epsilon^* = M' + iM''$ [25]. Solid-state NMR was employed for the molecular dynamics investigation by recording ^{13}C - ^1H rotor-encoded rotational echo double-resonance (REREDOR) spinning sideband patterns [27] at 243, 267, and 360 K for various recoupling times τ_{RC} of 40, 80, and 160 μs , and 25 kHz magic angle spinning (MAS) on a Bruker Avance 700 spectrometer using a standard double-resonance probe supporting rotors of 2.5 mm outer diameter. In addition, ^{13}C cross-polarization (CP) NMR spectra were recorded for the monocyno HBC as a function of temperature in the range 237–412 K. All experimental temperatures were corrected for the frictional heating effects [28].

The main effect of dipole substitution is to stabilize the columnar hexagonal liquid crystalline phase (Col_h) [29]. The WAXS images (Fig. 2) exhibit strong meridional reflections and a set of equatorial reflections with ratios $1:\sqrt{3}:\sqrt{4}$ relative to the primary peak. In addition, a weak reflection at intermediate distances is observed. The strong meridional reflection with a spacing of 0.36 nm (in the monocyno HBC) reflects intracolumnar distances while

the equatorial reflections are of intercolumnar origin. The weak reflection at intermediate distances indicates dipole-dipole correlations with an angle of about 90° as revealed by the azimuthal intensity distribution. From the T dependence of the corresponding meridional and equatorial reflections the corresponding intracolumnar and intercolumnar thermal expansion coefficients were extracted and found to be different ($\beta_{\text{intra}} \sim 7.6 \times 10^{-5} \text{ K}^{-1}$ and $\beta_{\text{inter}} \sim 1.35 \times 10^{-4} \text{ K}^{-1}$). The anisotropy in thermal expansivity originates from the anisotropic nature of the system composed from graphene discs and flexible hydrocarbon tails [16].

The analysis of the heteronuclear REREDOR NMR spinning sideband patterns (Fig. 2) provides site-specific information on the mobility. This is facilitated through the effective ^1H - ^{13}C dipole-dipole coupling constants D_{CH} , with the related local dynamic order parameters S representing the residual motional anisotropy of a given molecular segment [10]. S is given in terms of the second-order Legendre polynomial and is obtained experimentally as the ratio of the measured effective dipolar coupling constant to the dipolar coupling constant of a static pair:

$$S_{\text{CH}} = \left\langle \frac{1}{2} (3\cos^2\theta_{\text{CH}}(t) - 1) \right\rangle_t = \frac{\langle D_{\text{CH}}(t) \rangle_t}{D_{\text{CH,static}}} \quad (1)$$

For the monocyno HBC derivative a solid behavior is detected at temperatures below ~ 240 K, in agreement with the DSC T_g , where the aromatic core is practically frozen ($D = 21.0$ kHz, $S \rightarrow 1$). For the alkyl chains, the ^1H - ^{13}C dipole-dipole coupling constants of the CH_2 groups are reduced but to an average $D = 14.5$ kHz, $S = 0.69$, apart from the chain ends. In the Col_h mesophase, the ^1H - ^{13}C dipolar coupling constant for the aromatic CH moiety is reduced substantially due to the fast in-plane rotation [6,9,30]. Further reduction of the dynamic order parameter of the CH segment to $S = 0.42$ at 360 K is ascribed to out-of-plane disc excursions. The mean angle (38°) of this motion is obtained by assuming that the local dynamic order parameter S results from a Gaussian distribution of displacement angles [30]. At intermediate temperatures, the disc dynamics interferes with the frequencies in the kilohertz range pertinent to the NMR experiments. This leads to severely reduced ^{13}C signals in the CPMAS spectra (not shown). At the glass transition of organic glasses, the time scale of the molecular dynamics often exhibits a heterogeneous distribution of correlation times [31]. Indeed, such behavior is found here by recording ^{13}C - ^1H sideband patterns at an intermediate temperature of 267 K. For a short τ_{RC} of 40 μs , spectra of still frozen discs with $S \rightarrow 1$ are observed, whereas the spectrum for τ_{RC} of 160 μs gives $S = 0.42$, due to the fraction of mobile discs performing in-plane and out-of-plane motion (see Fig. 2). At this temperature, the two experimental time scales are at 10 and 0.1 s (see below). Thus, the faster DS process must correspond to the axial motion possessing a

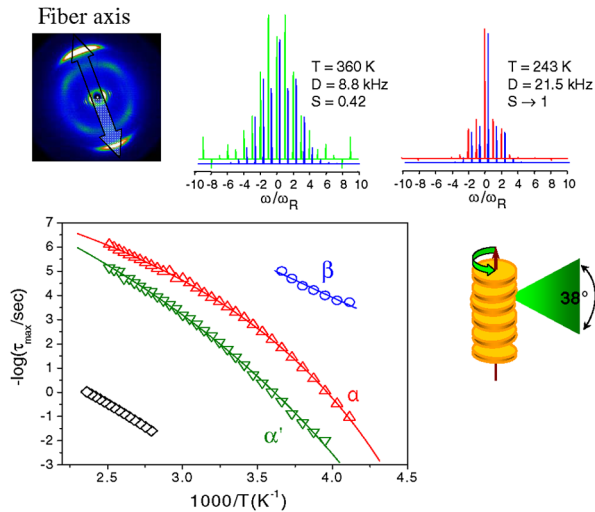


FIG. 2 (color online). Top: 2D-WAXS image of the monocyno HBC obtained from an oriented fiber ($T_{\text{extr}} = 273$ K) at 423 K revealing a columnar hexagonal liquid crystalline phase (Col_h) (left). ^{13}C - ^1H REREDOR spinning sideband patterns recorded at 25 kHz spinning at the magic angle and 360 K and 160 μs recoupling time (middle) and at 243 K and 40 μs recoupling time (right) with the simulated patterns [continuous (blue) lines] superimposed, resulting in local dynamic order parameters of $S = 0.42$ and 1, respectively. Bottom: Arrhenius relaxation map (left) for all dielectrically active processes and of the ionic mobility. Notice (i) the β process (circles) with an Arrhenius T dependence, (ii) the α (up triangles) and α' (down triangles) processes with VFT dependence, and (iii) the slow process (rhombus) due to the ionic mobility and the columnar structure indicating both in-plane and out-of-plane motions (right).

distribution of relaxation times. Indeed, for τ_{RC} of 80 μ s, the spectrum exhibits both features.

The corresponding time scales of this complex heterogeneous dynamics can best be studied by DS in the HBCs bearing strong dipole moments [monocyano ($\mu = 4.55$ D), monobromo ($\mu = 1.62$ D) and monoethynyl ($\mu = 0.25$ D)]. We discuss first the dynamics of the monocyano HBC bearing the strongest dipole moment. Three dielectrically active processes are detected associated with the cyano dipole relaxation and one process associated with the ionic mobility. The relaxation times of the different processes are shown in Fig. 2, in the usual Arrhenius representation. The low-temperature β process has an Arrhenius T dependence $\tau = \tau_0 \exp(E/RT)$, with a single activation energy $E = 55 \pm 5$ kJ/mol and a $\tau_0 = 4 \times 10^{-16}$ s, characteristic of a local process. Thus the β process is assigned to small-angle vibrational motions of the cyano group induced by the more mobile alkyl chains. At higher temperatures two processes exist, called α and α' , with a steeper temperature dependence that can be described by the Vogel-Fulcher-Tammann (VFT) equation

$$\tau = \tau_0 \exp\left(\frac{B}{T - T_0}\right) \quad (2)$$

where τ_0 is the relaxation time in the high T limit, B is the activation parameter, and T_0 is the “ideal” glass temperature. The B , T_0 , and T_g parameters assume the following values: 900 ± 23 K, 161 ± 2 K, and 237 ± 3 K for the α and 1730 ± 115 K, 128 ± 6 K, and 255 ± 6 K for the α' process. The characteristic relaxation times of the ion mobility (obtained from the crossing of the M' and M'') also display the common VFT dependence. Interestingly, the DSC T_g corresponds to the freezing of the DS α process (at $\tau \sim 10^2$ s). This process is less restricted and less volume demanding (see below with respect to the pressure dependence) and thus freezes at a lower temperature. Both processes are non-Debye with low (m)- and high- (mn)-frequency Havriliak-Negami slopes of $m = mn = 0.7$ (corresponding stretching exponent $\beta \sim 0.75$) and $m = mn = 0.4$ ($\beta \sim 0.45$) for the α and α' processes, respectively, and intensities of $T\Delta\epsilon \sim 240$ and 150 K. Clearly, the fast axial motion, as seen in NMR, leaves an uncompensated residual dipole moment as the dipole breaks the symmetry of the HBC disc and results in unevenly populated sites for the axial motion, stabilized by the dipole-dipole correlations of adjacent discs as revealed by WAXS. This residual dipole moment then relaxes through the slower (α') process with considerably lower relaxation strength. Combining the results of DS, NMR, and x rays, the α process reflects collective axial motions of the discs, which leaves a residual dipole with a defined average orientation within the column. The orientation correlation of the dipoles within the columns, however, has a limited lifetime and relaxes through highly collective

intracolumnar and perhaps intercolumnar rotational dynamics (α' process).

To explore further the origin of the slower process and to construct the phase diagram, we employ pressure as the additional relevant thermodynamic parameter. In these experiments, pressure is applied isothermally at temperatures where α and α' processes are probed within the experimental window (Fig. 3). Increasing pressure results in the slowing down of both processes, but remarkably there is a steeper P dependence for the slower α' process. The linear dependence of $\log\tau$ versus pressure can be used to define an apparent activation volume ΔV as $\Delta V = 2.303RT(\partial \log\tau/\partial P)_T$. This quantity is plotted in the inset of Fig. 3 as a function of the temperature difference from the respective T_g . Note that $\Delta V_{\alpha'} > \Delta V_{\alpha}$ indicating that pressure slows down more the highly collective slower process as compared with the less volume demanding axial motion of the discs.

Based on the T and P investigations a phase diagram can be constructed for the monocyano HBC that is depicted in Fig. 4. The two $T_g(P)$ dependencies corresponding to the freezing of the fast axial (α process) and of the slower collective reorganization (α' process) can be described by the empirical equation [25]:

$$T_g(P) = T_g(0) \left(1 + \frac{b}{c} P\right)^{1/b} \quad (3)$$

where b and c are fitting parameters [$b = 3.9$, $c = 540$ MPa, and $(dT/dP)_{P \rightarrow 0} = 0.44$ K/MPa for the α process and $b = 4.8$, $c = 370$ MPa, and $(dT/dP)_{P \rightarrow 0} = 0.69$ K/MPa for the α' process]. These dependencies separate the T - P phase space in three regimes depicted as glass I, glass II, and Col_h. As a result of the stronger pressure dependence for the slow collective reorganization, increasing pressure effectively stabilizes the glass II phase.

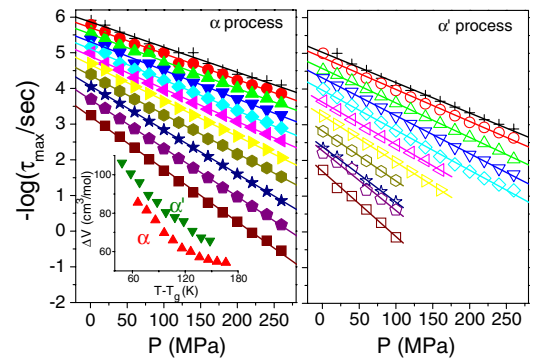


FIG. 3 (color online). Pressure dependence of the relaxation times at maximum loss corresponding to the α (left) and α' (right) processes of monocyano HBC. The symbols indicate temperatures in the range from 303 (squares) to 403 K (crosses) in steps of 10 K. The lines are the result of the fit giving rise to the apparent activation volume. Inset: Temperature dependence of the apparent activation volumes (ΔV) plotted as a function of the temperature difference from the respective T_g .

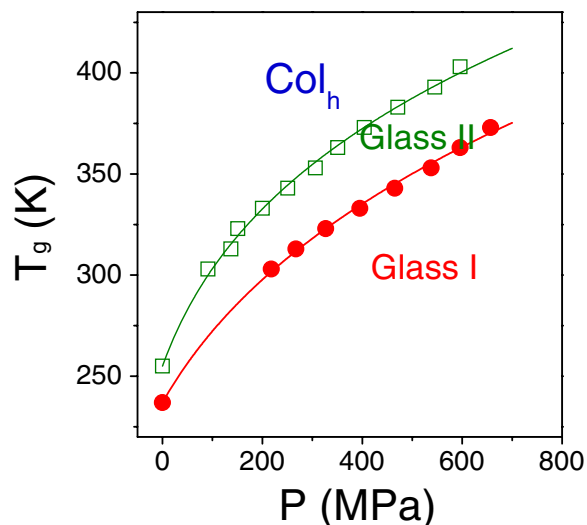


FIG. 4 (color online). “Phase diagram” for the monocyno HBC showing two “glass” phases and the columnar hexagonal liquid crystalline phase (Col_h) at higher temperatures. The lines are the result of the fit to Eq. (3).

Comparing the dynamics of all three functionalized HBCs we note that α and α' processes are clearly separated only for the HBCs bearing the stronger dipoles (monocyno and monobromo HBCs). In the monoethynyl HBC the peak shape is still asymmetric, yet deconvolution of the two processes is difficult. This is consistent with our assignment of the α' process, as the orientational correlation of the discs within the columns is expected to be more stable the stronger the dipole moment.

In conclusion, by employing static (x rays) and dynamic techniques (site-specific NMR and dielectric spectroscopy) it was possible to identify the liquid crystalline mesophase and the associated dynamics in a series of dipole functionalized HBCs. The combined NMR and DS investigations have shown unambiguously that the “fast” and “slow” dielectrically active processes are associated, respectively, with the axial disc motion and a collective reorganization of the columns that completely relaxes the dipole moment. The latter is particularly important to understand the alignment of the columns on surfaces [12] in the presence of electric field. All samples display similar dynamics within the Col_h phase suggesting that the thermodynamic state controls the dynamic response. The pressure investigation assists in identifying the slower dynamics and provides the first phase diagram for substances of this kind. Last, but not least, these results are supported by independent computer simulations along the lines described in Ref. [21].

This work was supported by DFG (SFB 625) and by the Greek GSRT (PENED 529 and 856). Discussions with

Dr. D. Andrienko and Professor K. Kremer are gratefully acknowledged.

*Corresponding author.

gfloudas@cc.uoi.gr

- [1] K. S. Novoselov *et al.*, Nature (London) **438**, 197 (2005).
- [2] J. Wu, W. Pisula, and K. Müllen, Chem. Rev. **107**, 718 (2007).
- [3] *Handbook of Liquid Crystals*, edited by D. Demus, J. Goodby, G.W. Gray, H.W. Spiess, V. Vill (Wiley-VCH, Weinheim, 1998).
- [4] W. Pisula *et al.*, Adv. Mater. **17**, 684 (2005).
- [5] A.M. van de Craats *et al.*, Adv. Mater. **11**, 1469 (1999).
- [6] J. Leisen, M. Werth, C. Boeffel, and H.W. Spiess, J. Chem. Phys. **97**, 3749 (1992).
- [7] M. Werth *et al.*, J. Phys. II (France) **3**, 53 (1993).
- [8] A. Hollander *et al.*, J. Phys. II (France) **6**, 1727 (1996).
- [9] P. Herwig, C. W. Kayser, K. Müllen, and H.W. Spiess, Adv. Mater. **8**, 510 (1996).
- [10] I. Fischbach *et al.*, J. Phys. Chem. B **106**, 6408 (2002).
- [11] S. U. Vallerien, M. Werth, F. Kremer, and H.W. Spiess, Liq. Cryst. **8**, 889 (1990).
- [12] D. Wasserfallen *et al.*, Adv. Funct. Mater. **15**, 1585 (2005).
- [13] M. Möller, J.H. Wendorff, M. Werth, H.W. Spiess, H. Bengs, O. Karthaus, and H. Ringsdorf, Liq. Cryst. **17**, 381 (1994).
- [14] M. Möller, J.H. Wendorff, M. Werth, and H.W. Spiess, J. Non-Cryst. Solids **170**, 295 (1994).
- [15] K. L. Ngai, J. Non-Cryst. Solids **197**, 1 (1996).
- [16] B. Glösen, A. Kettner, J. Kopitzke, and J.H. Wendorff, J. Non-Cryst. Solids **241**, 113 (1998).
- [17] Z. Yildirim *et al.*, J. Non-Cryst. Solids **351**, 2622 (2005).
- [18] O. Kruglova *et al.*, Chem. Phys. Chem. **8**, 1338 (2007).
- [19] G. J. Kearley *et al.*, Chem. Phys. **292**, 185 (2003).
- [20] F.M. Mulder *et al.*, J. Am. Chem. Soc. **125**, 3860 (2003).
- [21] D. Andrienko, V. Marcon, and K. Kremer, J. Chem. Phys. **125**, 124902 (2006).
- [22] J. Kirkpatrick, V. Marcon, J. Nelson, K. Kremer, and D. Andrienko, Phys. Rev. Lett. **98**, 227402 (2007).
- [23] P.G. de Gennes, J. Phys. Lett. **44**, 1 (1983).
- [24] A. Fechtenkötter *et al.*, Tetrahedron **57**, 3769 (2001).
- [25] G. Floudas, Prog. Polym. Sci. **29**, 1143 (2004).
- [26] P. Papadopoulos *et al.*, Macromolecules **37**, 8116 (2004).
- [27] K. Saalwächter and I. Schnell, Solid State Nucl. Magn. Reson. **22**, 154 (2002).
- [28] B. Langer, I. Schnell, H.W. Spiess, and A.-R. Grimmer, J. Magn. Reson. **138**, 182 (1999).
- [29] S. Ito *et al.*, Chem. Eur. J. **6**, 4327 (2000).
- [30] K. Schmidt-Rohr and H.W. Spiess, *Multidimensional Solid State NMR and Polymers* (Academic, New York, 1994).
- [31] K. Schmidt-Rohr and H.W. Spiess, Phys. Rev. Lett. **66**, 3020 (1991); U. Tracht *et al.*, Phys. Rev. Lett. **81**, 2727 (1998).